Sarunas MIKUCIONIS[1], Vytautas URBANAVICIUS[1], Antanas GURSKAS[1], Audrius KRUKONIS[1]

Vilnius Gediminas Technical University (1)

The Influence of the Air Gap on the Characteristics of the Double-Shielded Microstrip Delay Devices

Abstract. *A double-shielded microstrip (DSM) device is made of conventional microstrip device and by mounting additional shielded dielectric plate on top of it. The resulting structure is similar to the strip line, but there is a significant difference – a thin air gap that is equal to the thickness of the microstrip. The thickness of this air gap can become uncontrollable in the device manufacture process. In this paper the influence of thin air gap on the electrical parameters of DSM devices such as: microstrip line, coupled lines, multiconductor line, and meander delay line is investigated.*

Streszczenie. *W podwójnie ekranowanym mikropasku (DSM) układu opóźniającego DDs dodano dodatkową warstwę dielektryczną. Cienka szczelina powietrzna ma grubość paska. Ta szczelina może być trudna do kontrolowania w procesie produkcji. W artykule analizowano wpływ szczeliny powietrznej na parametry układu DSM .* ***Wpływ szczeliny powietrznej na właściwości podwójnie ekranowanego układu opóźniającego****.*

Keywords: Double-shielded microstrip device, air gap, meander delay line, effective permittivity, characteristic impedance.
Słowa kluczowe: podwójnie ekranowany mikropasek DSM, układ opóźniajacy

doi:10.12915/pe.2014.06.56

I. Introduction

Delay devices (DDs) are widely used in electronic systems for various purposes, e.g. to synchronize parallel transmitted signals [1], for real-time analogue signal processing [2], in antenna systems to shape a desired pattern [3] as well as a radiating element [4], in traveling wave devices for matching velocities of electromagnetic wave and the electron beam [5, 6], and as a substantial part in many other electronic devices [7, 8].

Currently, DDs based on active elements [9, 10] are popular, however, power consumption of active DDs is higher, and dynamic range is lower, besides bandwidth of such devices is more narrow. Electrodynamic DDs, such as helical [12] and meander [13] lines, don't exhibit these imperfections [11].

Meander devices are attractive because they can be implemented as small size and weight microstrip devices and therefore suitable for modern on-board and mobile telecommunication systems [14].

Microstrip devices are typically placed in a conductive package for protection against external electromagnetic fields. Top cover of such package becomes the second shield of the microstrip device. Beside that in case of microstrip DDs, e.g. meander delay line, additional dielectric plate is placed between the top shield and a microstrip conductor, in order to reduce overall dimensions, while maintaining retarding properties. The design of such microstrip DD becomes double-shielded (Fig. 1).

The resulting structure of the double-shielded device (Fig.1) is similar to a conventional stripline. However, one major difference is the presence of the air gap due to the non-zero thickness of the microstrip conductor. In order to distinguish such a structure from the conventional stripline, we call it *double-shielded microstrip* (DSM) structure. The said air gap makes the dielectric medium between the conductive shields inhomogeneous. In general, DSM device can be considered as a special case of a layered dielectric structure which is widely used in microwave engineering [15, 16] and intensively studied in the last decade [17–22]. Analysis of the effect of thin air gap on the electrical parameters of the DSM device is rather complicated. For example Kaifas and Sahalos [17] have researched properties of multiconductor lines in inhomogeneous bi-anisotropic media. Inhomogeneity in such a multiconductor line [17] can be formed by combining the dielectric layers and the air gap, but the upper shield in the proposed model is missing and this structure cannot be regarded as a double-shielded. Plaza *et al.* [18] have studied the DSM structures using quasi-TEM approach by hybrid technique that combines the method of lines (MoL) with the method of the moments. Despite the fact that the proposed model includes a top shield and so it is the double-shielded, the influence of the air gap on the properties of the DSM structures was not investigated here. Lucido [19] proposed a new spectral-domain analysis technique for analysis of single and multiple coupled microstrip lines in layered medium. The proposed model allows analysis of the influence of the air gap and the presence of the upper conductive shield on the properties of microstrip lines, but the finite thickness of microstrips is not taken into account in this model. Ymeri *et al.* [20] proposed procedure for capacitance matrix calculation of multilayer VLSI interconnects by using quasi-static analysis and Fourier series approach. In the proposed model, any combination of dielectric layers and thickness of the microstrips is taken into account, but the top shield is missing, so the model cannot be regarded as double-shielded. Shuing and Hanquing [21] combined two methods: the MoL with the finite-difference method (FDM) to calculate the capacitance and inductance matrices of the multiconductor lines in multilayer dielectric medium. Upper conductive shield was not considered in this model and this device is also not a double-shielded. Srivastava *et al.* [22] evaluated the dispersion characteristics of asymmetric multiconductor lines in shielded suspended substrate using hybrid-mode formulation. However, there was no dielectric plate between the conductors and the top shield in the proposed model and the effect of the air gap on the line parameters was not investigated.

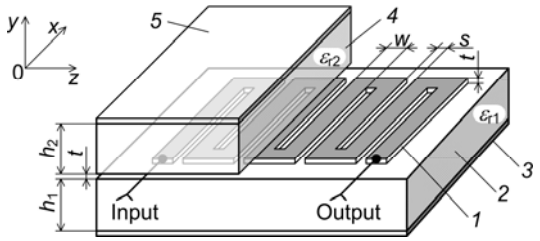

Fig. 1. The structure of the double-shielded microstrip meander delay line, where 1 is a signal conductor in the form of meander; 2 is a bottom dielectric substrate; 3 is a bottom shield; 4 is a dielectric plate; 5 is a top shield. Portion of the top plate is not shown here

Overview of open publications [17–22] reveals that the influence of the air gap on the performance of the DSM devices is still insufficiently studied and we will try to do it in this paper.

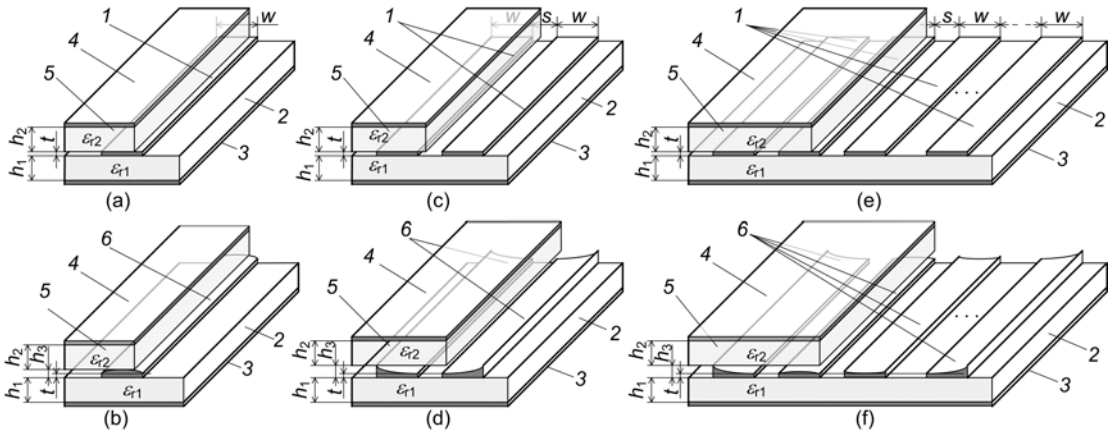

Fig. 2. The generalized structure of the double-shielded microstrip devices: transmission line (a), and transmission line with non-rectangular conductor (b), coupled microstrip lines (c), and coupled lines with non-rectangular conductors (d), multiconductor microstrip line (e), and multiconductor line with non-rectangular conductors (f) where 1 are rectangular microstrips; 2 and 5 are bottom and top dielectric substrates correspondently; 3 and 4 are bottom and top shields correspondently; 6 are the non-rectangular microstrips. Portion of the top dielectric plate and top shield are not shown here

II. Models of Double-Shielded Microstrip Devices

It was shown in the introduction that DSM devices are composed using conventional microstrip devices mounting over microstrips top dielectric plate with shield facing up. Examples of such DSM devices can be: transmission line, coupled microstrip lines, multiconductor line (Fig. 2), etc. DSM devices are different from stripline structures by having a thin air gap caused by the non-zero thickness of microstrips. It should also be noted that the thickness of the air gap may become unmanageable during the manufacture process of the DSM. The reason for this may be skewed upper dielectric plate at its installation or distortion of rectangular cross-section of microstrips during their formation. In Fig. 2 (b), (d) and (f) for illustration only possible distortions of microstrips rectangular cross-section are shown.

Up to now, the effective frequency range of the signals in microwave ICSs is still below 10 GHz. Therefore the quasi-TEM approach is still valid. The FDM is a flexible, efficient and well suited method for analysis of planar multilayered structure and multiconductor of arbitrary cross section. FDM and quasi-TEM approximation are used for the DSM devices modeling presented in this article.

III. Dependences of the Characteristics of the Double-Shielded Microstrip Devices on the Air Gap

The proposed models of the DSM devices were investigated in the following order. Firstly, accuracy of the mathematical model (the analysis stage) used in the proposed technique was tested. Next, the dependence of the effective permittivity $\varepsilon_{r\,eff}$, the characteristic impedance Z_0, and delay time t_d of the DSM devices on the air gap between top and bottom dielectric substrates were investigated. We investigated two kinds of dependences of electrical parameters of the DSM devices from the air gap: when the gap is emerged due to the non-zero thickness of the microstrips, and when the gap is emerged due to inaccurate mounting the upper dielectric plate.

A. Model Validation

A computer program has been developed to calculate all the parameters of the DSM devices. Here, for validation of the code, the effective permittivity and the characteristic impedance of the asymmetric four microstrip lines structure in suspended substrate are presented and compared in Figure 3 and Table 1, and good agreement exist between the calculated values and those reported in [22]. The maximum difference between the values that are obtained by our computer program and presented [22] does not exceed 3 percent in the most cases.

Table 1. Comparison parameters for four asymmetrically coupled microstrip lines in shielded suspended substrate* obtained using the proposed model (FDM), and in [22]

Conductor number	Mode A		Mode B		Mode C		Mode D	
	FDM	[22]	FDM	[22]	FDM	[22]	FDM	[22]
	Characteristic impedance [Ω]							
#1	117	120	68.8	70	41.2	40.18	28.1	27.73
#2	185	181	101	104	62.2	62.58	41.3	40.79
#3	250	242	145	146	79	77.6	53	52.06
#4	141	144	81.3	83	46.2	47.54	29.2	29.38

* Design parameters of this line are presented in Fig. 3.

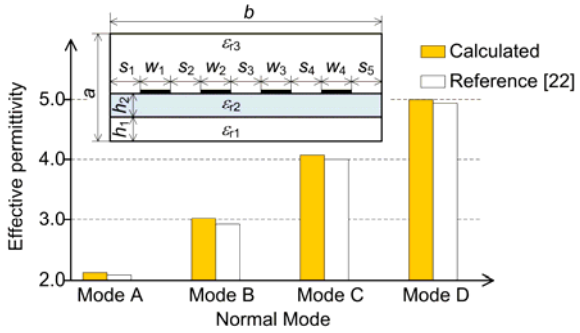

Fig. 3. Comparison plot of effective permittivity for four asymmetric coupled microstrip lines in shielded suspended substrate (w_1 = 0.5 mm, w_2 = 0.3 mm, w_3 = 0.2 mm, w_4 = 0.4 mm, s_2 = 0.3 mm, s_3 = 0.25 mm, s_4 = 0.2 mm, d = 0.254 mm, h_2 = 0.254 mm, s_1 = s_5, b = 12.07 mm, a = 5.254 mm, ε_{r1} = ε_{r3} = 1.0, ε_{r2} = 9.9)

B. Air Gap Due to non-zero Microstrips Thickness

Influence of the air gap, caused by the non-zero thickness of microstrips, on the effective permittivity and characteristic impedance of the DSM transmission line, coupled lines and six-conductor line is presented in Fig. 4 by corresponding curves. Two areas can be marked at all the curves: the initial region where the air gap emerges ($0 < t/h_1 < 0.005$) and the region where it further increases ($t/h_1 > 0.005$). It is seen that with increasing microstrips thickness from 0 to $t/h_1 = 0.005$ all the curves change abruptly. Such a drastic change of the effective permittivity and the characteristic impedance is due to a shift of the distribution of the electric field in the cross-section of investigated devices. When the air gap is absent, the structure of such devices corresponds to the stripline structure and electric field is fully concentrated in the dielectric area. As a result, the

effective permittivity is equal to the dielectric constant of the substrate, so capacitance per-unit-length of lines is relatively large and impedance correspondently is small. As soon as a thin layer of air emerges ($0 < t/h_1 < 0.005$ in our case), the structure of the investigated device from stripline becomes double-shielded microstrip. Part of the electric field lines pass from the dielectric to the air, because of this there is a sharp decrease of the effective permittivity and lines capacitance per-unit-length and thus the impedance increases. With further increase of the microstrips thickness and the air gap ($t/h_1 > 0.005$), more and more electric field lines pass through the air and the effective permittivity decreases further (Fig. 4 (a), (c) and (e)). It should be noted that the expected increase of the characteristic impedance here is not observed – on the opposite, it decreases. This decrement of the characteristic impedance can be explained by accumulation of the additional electric charge on the increasing side walls of microstrips and, as a consequence, by increment of their capacitance per-unit-length.

Fig. 4 (c)–(f) shows the change of effective permittivity and characteristic impedance of the DSM coupled lines and six-conductor multiconductor DSM line for the even and odd modes. It should be noted that the effective permittivity (Fig. 4 (c) and (e)) of the odd mode is more sensitive to changes of the air gap due to the fact that more of the electric field lines are concentrated in this gap than in the even mode case. Characteristic impedance (Fig. 4 (d) and (f)) in this instance varies considerably less and almost in the same manner for the even and odd modes. It should be also noted that despite the considerable qualitative changes of the effective permittivity and the characteristic impedance shown in Fig. 4, when the air gap emerges and increases, the relative variations of these parameters are not so significant. For example, the discussed jump of all curves in the initial area, when the air gap emerges, does not exceed 2%–4%, and even twentyfold increase of the gap (from to $t/h_1 = 0.005$ to $t/h_1 = 0.1$) does not cause variation curves by more than 2%–6%.

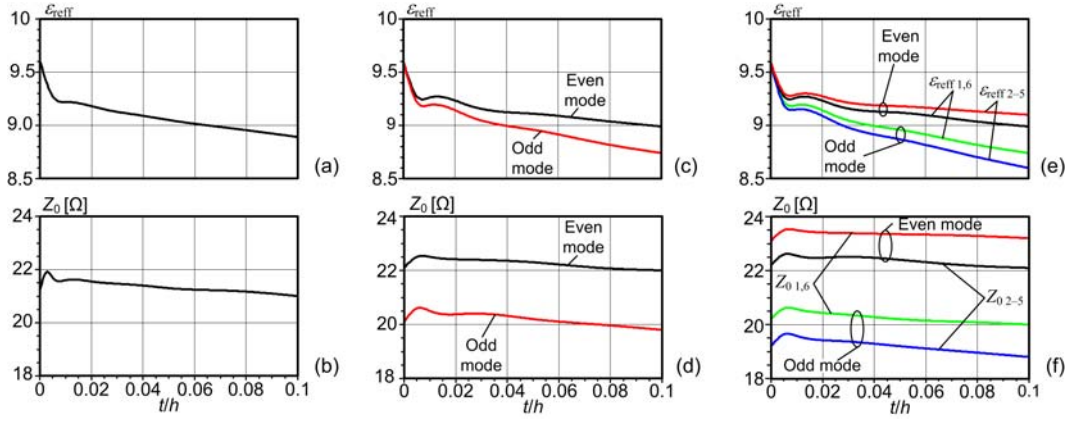

Fig. 4. Effective dielectric permittivity and characteristic impedance of double-shielded microstrip structures: transmission line ((a) and (b)), coupled lines ((c) and (d)), six-conductors line ((e) and (f)) vs. normalized air gap formed by the finite thickness of microstrips ($\varepsilon_{r1} = \varepsilon_{r2} = 9.6$, $w_i/h_1 = 2.0$, $s_i/h_1 = 1.0$, $h_2/h_1 = 1.0$, $h_1 = 0.5$ mm)

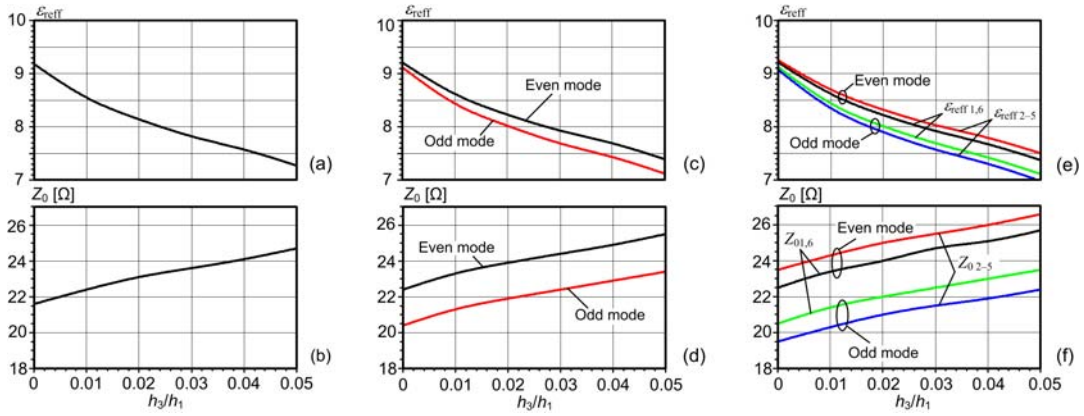

Fig.5. Effective dielectric permittivity and characteristic impedance of double-shielded microstrip structures: microstrip line (a) and (b), coupled lines (c) and (d), six conductors multiconductor line (e) and (f) vs. normalized air gap thickness ($\varepsilon_{r1} = \varepsilon_{r2} = 9.6$, $w_i/w_1 = 1.0$, $w_1/h_1 = 2.0$, $s/h_1 = 1.0$, $t/h_1 = 0.02$, $h_2/h_1 = 1.0$, $h_1 = 0.5$ mm)

C. Air Gap above the Microstrips

When the upper dielectric plate is mounted imprecisely, the air gap of the DSM devices is further increased. The impact of this increased gap on the effective permittivity and characteristic impedance of the DSM transmission line, coupled lines and six-conductor line is presented in Fig. 5 by corresponding curves. Here it is seen that the effective permittivity and characteristic impedance of the investigated devices are varied monotonously when the air gap is changed – no jumps of curves noticed. However a quantitative change of the permittivity and impedance is greater than in the case of the gap caused by the non-zero microstrips thickness only. For example, for almost threefold increase of the total air gap (the entire horizontal axis of Fig. 5) the effective permittivity changes within 21%–23% (Fig. 5 (a), (c), and (e)), and the characteristic impedance – 13%–14% (Fig. 5 (b), (d), and (f)). Such a significant change of the permittivity and impedance may be clarified that now the layer of air is in contact not only with microstrips side walls but also is located between the microstrips plane and the upper dielectric plate, so the electric field in this area is passed from the dielectric medium into the air space and the lines capacitance per-unit-length decreases.

D. Double-Shielded Microstrip Meander Delay Line

In order to investigate the influence of the air gap on the frequency dependence of the phase delay (i.e., the dispersion characteristics) of DSM meander delay line (DSMMDL) two models were created. The first model (Fig. 1) takes into account the influence of the air gap caused by the non-zero thickness meander microstrips. The gap between the meander and upper dielectric plate is absent here. The second model imitates deviated mounting of dielectric plate on top of the DSMMDL resulting in an additional air gap above the meander conductor. The calculated dispersion characteristics of the DSMMDL are presented in Fig. 6. The DSMMDL models are formed from multiconductor line, parameters of which are shown in Fig. 4 (e), (f) and in Fig. 5 (e), (f). The length 2*A* of the meander strips in this case is chosen to be equal to 100 mm. The calculations are performed in two ways: a hybrid method – a combination of the FDM and scattering matrices [11] (authors' developed software), and using Sonnet® simulator. The curves in Fig. 6 (a) show the effect of the thickness of the air gap, which is caused by the non-zero thickness of meander microstrips on the dispersion characteristics of the DSMMDL.

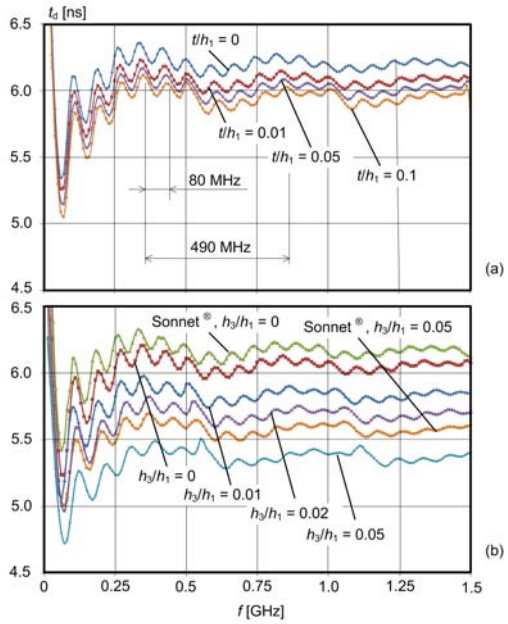

Fig. 6. Calculated and simulated dependencies of dispersive characteristics of the DSM meander delay line on conductor thickness (a) and thickness of the air gap (b). ($\varepsilon_{r1} = \varepsilon_{r2} = 9.6$, $w_i/w_1 = 1.0$, $w_1/h_1 = 2.0$, $s/h_1 = 1.0$, $t/h_1 = 0.02$, $h_2/h_1 = 1.0$, $h_1 = 0.5$ mm)

Fig. 6 (b) displayed the same characteristics, but their variation along the time axis due to changes of the air gap above the meander conductor. Chart analysis shows that at very low frequencies there is a significant rise of the dispersion characteristics inherent in all meander delay lines. However, despite the large absolute values of this rise, the ratio of the delay time with the period of the correspondent low-frequency oscillation is only a fraction of a percent, and does not cause significant phase distortion. At all the dispersion characteristics of Fig. 6 oscillations of two types are visible: of a rare repetition period along the frequency axis – about 0.5 GHz, and with the frequent repetition period – about 80 MHz. The assumption can be made that rare oscillations (0.5 GHz) are caused by inhomogeneities of the signal path at the ends of the meander strips where neighbour strips are connected with each other (0.48–0.55 GHz, depending on the thickness of the air gap, is the frequency at which the coupled neighbour strips are a wavelength long). Frequent oscillations are due to inhomogeneities on input and output terminals of the DSMMDL. Their repetition period corresponds to half the value of the resonant frequency of the entire DSMMDL (from 160/2 = 80 MHz till 180/2 = 90 MHz).

Analysis of the dispersion characteristics (Fig. 6 (a)) shows that when the air gap emerges in the stripline structure due to the finite microstrips thickness (i.e. stripline becomes DSM), delay time of the DSMMDL reduces by about 2.5 %, and a further increase of this gap has almost no effect on the delay time. For example, when the thickness of this gap increases tenfold the delay time decreases by only 1.7 %. The air gap above a meander conductor has more influence on the absolute values of the dispersion characteristics has (Fig. 6 (b)). Here it is seen that a fivefold increase of the air gap (from $h_3/h_1 = 0.01$ till $h_3/h_1 = 0.05$) reduces the delay time of about 9 %.

Fig. 6 (b) also shows the dispersion characteristics calculated using Sonnet® simulator. Here it is seen that the difference between the characteristics obtained by our hybrid method and the simulator do not exceed 3 %.

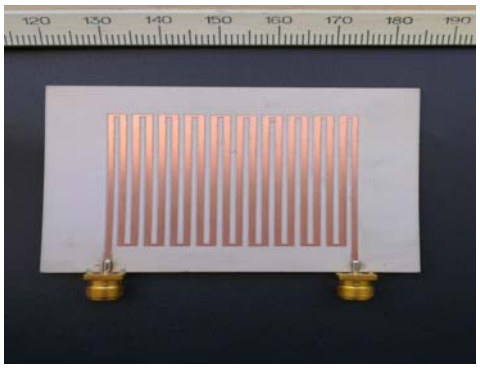

Fig. 7. Prototype of the double-shielded microstrip meander delay line (before the top dielectric plate mounting). Design parameters of the prototype are: $\varepsilon_{r1} = \varepsilon_{r2} = 6.15$, $w = 1.1$ mm, $h_1 = h_2 = 1.27$ mm, $s = 1.0$ mm, $t_1 = 0.035$ mm, $2A = 50$ mm, Number of the meander strips $N = 20$.

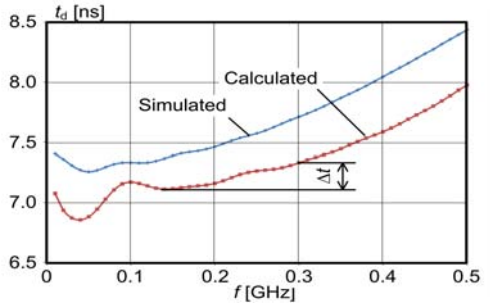

Fig. 8. Calculated and simulated dispersive characteristics of the DSM meander delay line prototype

IV. Experimental Measurements

Prototype of the DSM meander delay line was designed, constructed (Fig. 7) and measured to confirm the adequacy of the proposed models of the DSM devices. The prototype was made on the dielectric substrate Rogers® 3006, its dimensions and topology of the meander are presented in the title of Fig. 7. Calculated dispersion characteristic of the DSMMDL prototype is shown in Fig. 8. The dispersion characteristic simulated by Sonnet® is shown here also. The relative difference between them does not exceed 6 %. It is seen in Fig. 8 that prototype bandwidth determined with the proviso that phase distortion does not exceed 0.35 rad, using the equation:

$$\Delta F = 0.35/(2\pi\Delta t) \quad (1)$$

where Δt is deviation of dispersion characteristic on the boundary of the bandwidth from its value in the middle of the bandwidth, is equal to 300 MHz. Phase delay of the DSMMDL, calculated according to proposed DSM device model, in the middle of the bandwidth equals 7.1 ns.

Prototype measurements were performed in the time domain using sampling oscilloscope PicoScope 9312 from Pico Technology Ltd. Waveforms of the input and output voltage transients of the measured DSMMDL prototype are shown in Fig. 9. It is seen here that the rise time of the output transient between the levels of 0.1 and 0.9 is 1.2 ns and equivalent bandwidth of DSMMDL calculated according to equation:

$$\Delta F = 0.35/\tau_{\mathrm{t}} \tag{2}$$

where τ_{t} is the rise time the output transient, corresponds to 300 MHz. Averaged measured delay time between input and output transients at 0.5 levels equals 7.094 ns, which demonstrates a very good agreement with the calculated phase delay (7.1 ns).

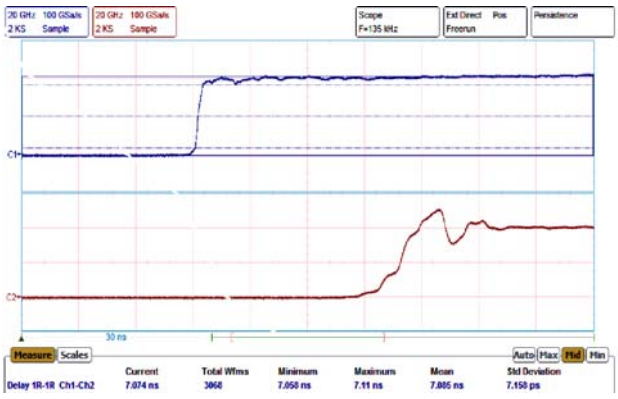

Fig. 9. Measured transients on the input (top) and output (bottom) of the double-shielded microstrip meander delay line. Measured delay parameters, shown on the bottom are: "Current" – 7.074 ns, "Minimum" – 7.058 ns, "Maximum" – 7.11 ns, "Mean" – 7.094 ns, "Std. Deviation" – 7.158 ps,

IV. Conclusion

Models of the double-shielded microstrip (DSM) delay devices, based on a combination of the finite difference method and the scattering matrix technique, are proposed in this paper. It is shown here that the presence of the uncontrolled air gap in these devices can significantly affect their parameters. For example, the air gap of only 25 micrometers can reduce the nominal value of phase delay of the DSM meander delay line by more than 10 %. The manufactured and measured prototype of the DSM meander delay line and simulation results confirmed the adequacy of the proposed models.

The authors wish to express their gratitude to the Rogers Corporation for the samples of the dielectric substrates, and the JSC "ELTESTA" for help with the measurements.

REFERENCES

[1] Hsu H., Wen J.H., Timing Synchronization in Ultra-Wideband Systems with Delay Line Combination Receivers, *Communications Letters, IEEE*, 11 (2007), No. 3, 264–266

[2] Gupta S., et al, CRLH–CRLH C-Section Dispersive Delay Structures with Enhanced Group-Delay Swing for Higher Analog Signal Processing Resolution, *IEEE Transactions on MTT*, 60 (2012), No. 12, 3939–3949

[3] Chu T.-S., Hashemi H., True-Time-Delay-Based Multi-Beam Arrays, *IEEE Transactions on MTT*, 61 (2013), No. 8, 3072–3082

[4] Kuo Y.-H.,et al., A Digital-Calibrated Transmitter-to-Receiver Isolator in Radar Applications, *IEEE Microwave and Wireless Components Letters*, 22 (2012), No. 12, 651–653

[5] Xu L., Yang Z.-H., Li J.-Q., Li B., 3-D Finite-Element Eigenvalue Analysis of Slow-Wave Structures of Traveling-Wave Tubes Without Matching Meshes, *IEEE Transactions on MTT*, 61 (2013), No. 10, 3524–3528

[6] Daskevicius V., et al, Simulation and Properties of the Wide-Band Hybrid Slow-Wave System, *Electronics and Electrical Engineering*, (2010), No. 104(8), 43–46

[7] Li G., et al, Delay Line Based Analog-to-Digital Converters, *IEEE Transactions on Circuits and Systems-II. Express Briefs*, (2009), No. 6, 464–468

[8] ŠIMKO M., CHUPAČ M., The theoretical synthesis and design of symmetrical delay line with surface acoustic wave for oscillators with single-mode regime of oscillation, *PRZEGLĄD ELEKTROTECHNICZNY (Electrical Review)*, 88 (2012), No. 12a, 347–350

[9] Wu C.-T. M., et al, *A* Dual-Purpose Reconfigurable Negative Group Delay Circuit Based on Distributed Amplifiers, *Microwave and Guided Wave Letters*, 23 (2013), No. 11, 593–595

[10] Kim H., et all., A 0.25-um BiCMOS feed forward equalizer using active delay line for backplane communication, *IEEE International Symposium on Circuits and Systems ISCAS 2007*, (2007), 193–196

[11] Staras S., et al, *Wide-Band Slow-Wave Systems: Simulation and Applications*, CRC Press, pp. 438, 2012

[12] Katkevičius A., et al, Calculations of characteristics of microwave devices using artificial neural networks, *PRZEGLĄD ELEKTROTECHNICZNY (Electrical Review)*, 88 (2012), No. 1a, 281–285

[13] Metlevskij E., Urbanavicius V., Analysis of charge distribution on rectangular microstrip structures, *Acta Physica Polonica A*, 119 (2011), No. 4, 503–508

[14] Lai C.-H., et al., Microwave Three-Channel Selector Using Tri-Mode Synthesized Transmission Lines, *IEEE Transactions on MTT*, 61 (2013), No. 10, 3529–3540

[15] Périgaud A., et al, Synthesis of Vertical Interdigital Filters Using Multilayered Technologies, *IEEE Transactions on MTT*, 60 (2012), No. 4, 965–974

[16] Ta H. H., Pham A-. V., Dual Band Band-Pass Filter With Wide Stopband on Multilayer Organic Substrate, *IEEE Microwave and Wireless Components Letters*, 23 (2013), No. 4, 193–195

[17] Kaifas T. N., Sahalos J. N., Multiconductor Transmission Lines in Inhomogeneous Bi-Anisotropic Media, *IEEE Transactions on MTT*, 56 (2008), No. 3, 638–653

[18] Plaza G., Marques R., Medina F., Quasi-TM MoL/MoM Approach for Computing the Transmission-Line Parameters of Lossy Lines, *Transactions on MTT*, 54 (2006), No. 1, 198–209

[19] Lucido M., A New High-Efficient Spectral-Domain Analysis of Single and Multiple Coupled Microstrip Lines in Planarly Layered Media, *IEEE Transactions on MTT*, 60 (2012), No. 7, 2025–2034

[20] Ymeri H., Nauwelaers B., Maex K., Efficient procedure for capacitance matrix calculation of multilayer VLSI interconnects using quasi-static analysis and Fourier series approach, *Journal of Telecommunications and Information Technology*, (2002), No. 2, 40–45

[21] Shujing L., Hanqing Z., An Efficient Algorithm for the Parameter Extraction of Multiconductor Transmission Lines in Multilayer Dielectric Media, *Digest on Antennas and Propagation Society International Symposium, 2005 IEEE*, 3A (2005), No. 3, 228–231

[22] Srivastava K.V., Awasthi S., Biswas A., Dispersion and Attenuation Characteristics of Asymmetric Multiconductor Lines in Suspended Substrate Structure Using Full-Wave Modal Analysis, *Microwave and Optical Technology Letters*, 48 (2006), No. 7, 1305–1310

Authors: *PhD. Student Sarunas Mikucionis, sarunas.mikucionis@dok.vgtu.lt, Prof. Dr. (HP) Vytautas Urbanavicius, vytautas.urbanavicius@vgtu.lt, Assoc. Prof. Dr. Antanas Gurskas, antanas.gurskas@vgtu.lt, Lector Dr. Audrius Krukonis, audrius.krukonis@vgtu.lt, Department of Electronic Systems, Faculty of Electronics, Vilnius Gediminas Technical University, Naugarduko str. 41-425, LT – 03227, Vilnius, Lithuania.*